Matter and Radiation at Extremes | RESEARCH ARTICLE | scitation.org/journal/mre

Theoretical investigations on x-ray transport in radiation transport experiments on the Shenguang-III prototype laser facility

Cite as: Matter Radiat. Extremes 7, 025901 (2022); doi: 10.1063/5.0043745
Submitted: 11 January 2021 • Accepted: 20 December 2021 •
Published Online: 25 January 2022

Guangwei Meng,[1,a] Jun She,[1,a] Tianming Song,[2] Jiamin Yang,[2] and Min Wang[1]

AFFILIATIONS

[1]Institute of Applied Physics and Computational Mathematics, P.O. Box 8009, Beijing 100088, People's Republic of China
[2]Research Center of Laser Fusion, Mianyang 621900, People's Republic of China

[a]Authors to whom correspondence should be addressed: meng_guangwei@iapcm.ac.cn and she_jun@iapcm.ac.cn

ABSTRACT

Experiments exploring the propagation of heat waves within cylindrical CH foams were performed on the Shenguang-III prototype laser facility in 2012. In this paper, the radiation fluxes out of CH foam cylinders at different angles are analyzed theoretically using the two-dimensional radiation hydrodynamics code LARED-R. Owing to the difficulty in validating opacity and equation of state (EOS) data for high-Z plasmas, and to uncertainties in the measured radiation temperature T_r and the original foam density ρ_0, multipliers are introduced to adjust the Au material parameters, T_r, and ρ_0 in our simulations to better explain the measurements. The dependences of the peak radiation flux $F_{\max}$ and the breakout time of the heat wave t_{half} (defined as the time corresponding to the radiation flux at half-maximum) on the radiation source, opacity, EOS, and ρ_0 scaling factors (η_{src}, η_{op}, η_{eos}, and η_ρ) are investigated via numerical simulations combined with fitting. Then, with the uncertainties in the measured T_r and ρ_0 fixed at 3.6% and 3.1%, respectively, experimental data are exploited as fiducial values to determine the ranges of η_{op} and η_{eos}. It is found that the ranges of η_{op} and η_{eos} fixed by this experiment overlap partially with those found in our previous work [Meng *et al.*, Phys. Plasmas **20**, 092704 (2013)]. Based on the scaled opacity and EOS parameters, the values of $F_{\max}$ and t_{half} obtained via simulations are in good agreement with the measurements, with maximum errors ~9.5% and within 100 ps, respectively.

I. INTRODUCTION

Radiation transport is of crucial importance to high-energy-density physics (HEDP)[1,2] and is a fundamental energy transport mechanism in inertial confinement fusion (ICF)[3] and in many laboratory and astrophysical plasmas.[4–8] In indirect drive ICF, a high-Z hohlraum is used to convert large amounts of laser energy into high-temperature x-rays, which are then absorbed by the ablator of a fusion capsule through radiation transport, with radiation hydrodynamic behavior ensuing. In the astrophysical field, many phenomena, such as radiative shocks[9] and nebulae with dense, cool star-forming regions irradiated by nearby stars,[10] are correlated with radiation transport.

Over recent decades, a number of theoretical[11–15] and experimental[16–21] investigations focusing on radiation transport have been conducted. From a theoretical aspect, Hammer and Rosen[11] have developed a perturbation technique for solving the nonlinear radiation diffusion equation for both the supersonic and subsonic cases. Quantities of practical interest, such as the depth of heat front penetration and the absorbed heat flux, can be readily derived with their method. In our previous work,[12] a theoretical method was proposed to verify the opacity and equation of state (EOS) of high-Z plasmas in rarefactive states, based on two independent experimental measurements, namely, the propagation of heat waves and hydrodynamic motion in radiation ablation processes. From an experimental aspect, Back *et al.*[16] have performed experiments on low-density (40–50 mg/cm^3) foams to study diffusive supersonic radiation transport, where the ratio of the diffusive radiation front velocity to the material sound speed exceeds 2, using the Omega laser facility. Guymer *et al.*[17] have carried out supersonic diffusive radiation flow experiments on the National Ignition Facility (NIF), aiming at exploring the radiation flow through optically thick media from a strong radiation source.

The propagation of heat waves within CH foam cylinders was explored experimentally on the Shenguang-III prototype laser facility in 2012. Compared with the experimental works in Refs. 16–21, the heat wave in the foam was nondiffusive in this experiment, and the foam became optically thin after it had been completely heated by the radiation. Furthermore, the radiation fluxes out of the CH foam were measured simultaneously at different angles in each shot, which gave a more detailed characterization of the radiation transport process in the foam. The experiment was designed to obtain accurate data on heat wave propagation, so that we could study the effect of the Au sleeve on the heat wave propagation and validate our two-dimensional (2D) radiation hydrodynamic code. A schematic of the targets for the experiments, consisting of a half-hohlraum (referred to as a "halfraum" in this paper), a glint shield, and a foam sample, is displayed in Fig. 1. In the experiments, the 800 μm long Au halfraum with a diameter of 1000 μm was illuminated through a laser entrance hole (LEH) with a diameter of 800 μm by square pulses from one end, delivering an energy of ~6 kJ in 1 ns. The laser wavelength was 0.35 μm. The generated x-rays, with a peak radiation temperature $T_r \approx 240$ eV, were delivered into the cylindrical CH foam, driving a supersonic heat wave within it. A glint shield composed of 0.1 μm thick Au foil and 1 μm thick CH foil was placed between the halfraum and the foam sample with the purpose of eliminating any reflected laser that might preheat the foam. The CH foam cylinders at 19.9 mg/cm^3 (uncertainty ~3.1%), with lengths 1000 and 1500 μm and diameter 1000 μm, were surrounded with a 20 μm thick Au sleeve.[22] The radiation fluxes out of the CH foam cylinders at different angles (45°, 56°, and 67°) relative to the foam cylinder axis were measured using flat-response x-ray detectors (FXRDs).[23,24] The T_r at 20° relative to the halfraum axis was measured from the LEH using a soft x-ray spectrometer (SXS).

In this paper, we analyze the radiation fluxes out of the foam using the two-dimensional (2D) radiation hydrodynamic code LARED-R.[25,26] Since it is difficult to validate opacity and EOS data for high-Z plasmas, and uncertainties exist in the measured T_r and the original foam density ρ_0, multipliers are introduced to adjust the Au material parameters, T_r, and ρ_0 in our simulations to better explain the measurements. The dependences of the peak radiation flux $F_{\max}$ and the breakout time of the heat wave t_{half} (defined as the time corresponding to the radiation flux at half-maximum) on the radiation source, opacity, EOS, and ρ_0 scaling factors (η_{src}, η_{op}, η_{eos}, and η_ρ) are investigated via numerical simulations combined with fitting. Then, with the uncertainties in the measured T_r and ρ_0 fixed at 3.6% and 3.1%, respectively, the ranges of η_{op} and η_{eos} are determined using experimental data as fiducial values and are compared with those presented in our previous work.[12] Finally based on the scaled opacity and EOS parameters, $F_{\max}$ and t_{half} obtained via simulations are found to be fairly consistent with the measurements, with maximum errors ~9.5% and within 100 ps, respectively.

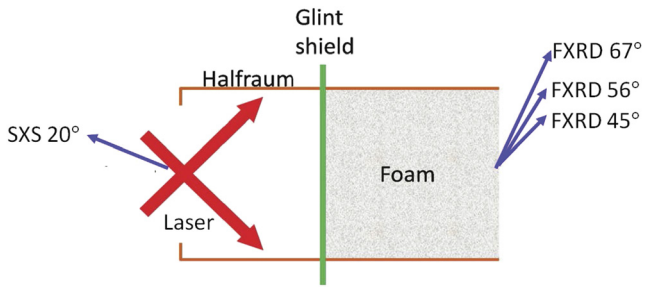

FIG. 1. Schematic of the targets for the experiments.

The remainder of this paper is organized as follows. In Sec. II, we briefly describe the simulation code LARED-R and the computational model employed in this study. In Sec. III, an analyses and discussion of the experimental results are presented. Finally, in Sec. IV, concluding remarks are made.

II. MODEL AND METHOD

The propagation of the heat wave within the foam sample is simulated using the LARED-R code, which is a 2D Lagrangian radiation hydrodynamic code in cylindrical geometry. It code includes three kinds of radiative models: multigroup radiative diffusion, multigroup radiative transfer, and multigroup radiative transfer and diffusion coupling. The electrons and ions are assumed to be in respective local thermodynamic equilibrium (LTE) states, with individual temperatures T_e and T_i.

In our simulations, the heated glint shield and CH foam cylinders, which are optically thin, are simulated based on the multigroup radiative transfer model. The Au sleeve is always optically thick and is simulated using the multigroup radiative diffusion model. The opacity data for Au and CH plasmas are obtained using the OPINCH code,[27] based on a relativistic Hartree–Fock–Slater (HFS) self-consistent average atom model.

The EOS data for CH and Au plasmas are extracted from the quotidian equation of state (QEOS)[28] and our unpublished internal scientific report, respectively. The independent thermodynamic variables in the Au EOS are the density and the temperature. The ions are treated as an ideal gas with pressure p_i and specific internal energy ϵ_i given by

$$p_i = \Gamma_i \rho T_i, \tag{1}$$

$$\epsilon_i = c_{vi} T_i, \tag{2}$$

where ρ is density, T_i is ion temperature, c_{vi} is the ion specific heat at constant volume, and $\Gamma_i = \frac{2}{3} c_{vi}$. The electron EOS is derived from a real gas model. The electron pressure p_e and specific internal energy ϵ_e are given by

$$p_e = D\left(\frac{\rho}{\rho_c}\right)^n T_e^m, \tag{3}$$

$$\epsilon_e = B\left(\frac{\rho}{\rho_c}\right)^{-l} T_e^m, \tag{4}$$

where T_e is the electron temperature, ρ_c is the normal density of the material, and D, B, n, m, and l are constants related to the material.

III. RESULTS AND DISCUSSION

First, in Sec. III A, we describe the radiation source in our simulations, present the simulation results calculated with LARED-R using the original Au material parameters, and discuss the possible physical factors resulting in discrepancies between simulations and

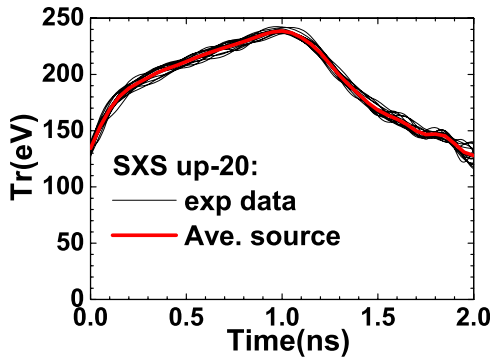

FIG. 2. Time profiles of T_r at 20° relative to the halfraum axis. The black solid lines show time profiles of T_r measured with the SXS from different shots. The red solid line shows the average T_r of these shots.

experiments. Second, in Sec. III B, we investigate the dependences of F_{max} and t_{half} on the radiation source, opacity, EOS, and ρ_0 scaling factors (η_{src}, η_{op}, η_{eos}, and η_ρ) by combining simulations with fitting. Then, with the uncertainties in the measured T_r and ρ_0 fixed at 3.6% and 3.1%, respectively, we determine the ranges of η_{op} and η_{eos} by using experimental data as fiducial values. Finally, simulation results based on the scaled Au material parameters are presented and compared with the experiments.

A. Simulation results using the original Au material parameters

In the experiments, the laser-heated Au halfraums provided a time-dependent radiation source, which drove supersonic heat waves within the CH foam cylinders. In our simulations, the glint shield, the CH foam cylinder, and the Au sleeve are treated as a system, and the radiation source is applied at the boundary of the glint shield as a surface source. The source is fixed in space during the heat wave propagation. Time profiles of T_r at 20° measured by the SXS from the LEH are shown in Fig. 2. The black solid lines show time profiles of T_r measured in different shots. The average T_r of these shots, shown by the red solid line, is used as the radiation source in the following simulations. The standard deviation of the peak T_r measured in different shots is 0.7%. The systematic error in the flux measurement is about 15% of the peak flux, corresponding to a systematic error of 3.5% in T_r. Thus, the total uncertainty in T_r is calculated from the two kinds of errors as $\sigma = \sqrt{(0.7\%)^2 + (3.5\%)^2} = 3.6\%$.

Figure 3 shows a comparison of the radiation fluxes out of the 1000 μm [(a)–(c)] and 1500 μm [(d)–(f)] foam cylinders at 45°, 56°, and 67° between the measurements from different shots (shown in black) and simulated results derived from the original radiation source and Au material parameters (shown in red). The gray regions show the measurement errors for the time and fluxes, which are about 100 ps and 15% of the peak flux, respectively.[23] It is found that the simulated results do not match the measurements very well. The simulated F_{max} is generally smaller than the experimental data. The

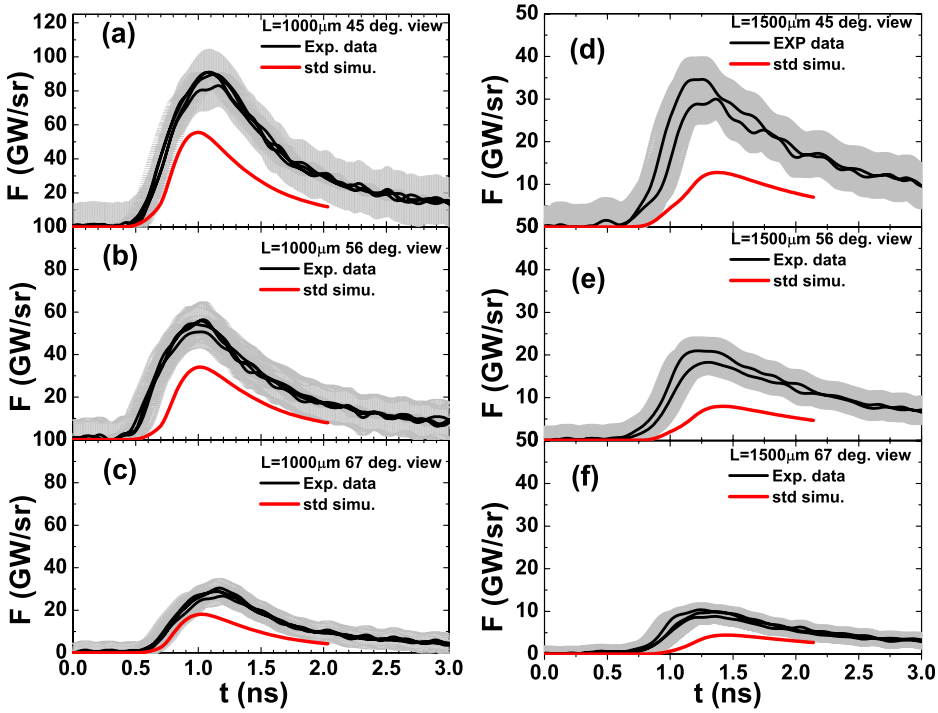

FIG. 3. Comparison of the radiation fluxes out of the 1000 μm [(a)–(c)] and 1500 μm [(d)–(f)] foam cylinders at (a) and (d) 45°, (b) and (e) 56°, and (c) and (f) 67° between the measurements from different shots (shown in black) and simulated results derived from the original radiation source and Au material parameters (shown in red). The measurement errors of the time and fluxes are shown by the gray regions.

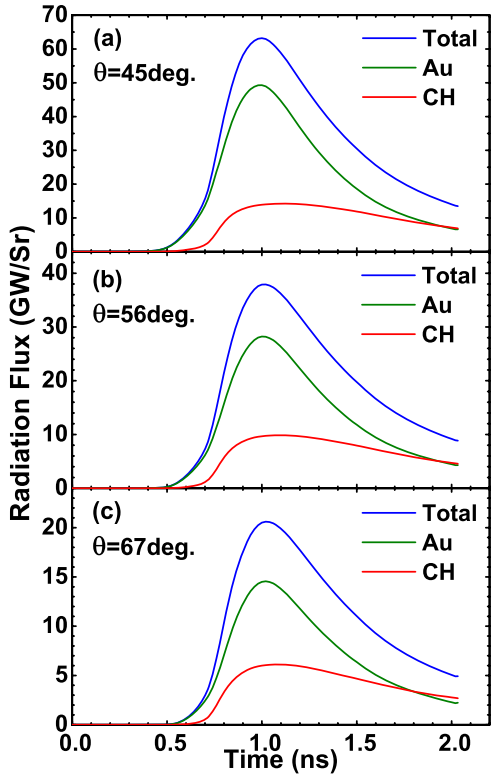

FIG. 4. Time profiles of the radiation fluxes emitted by the Au plasma (green solid line), CH plasma (red solid line), and the entire foam cylinder (blue solid line) at (a) 45°, (b) 56°, and (c) 67° for a 1000 μm foam cylinder.

simulated t_{half} at 45° and 67° for the 1000 μm foam is consistent with experimental data, but the other simulated t_{half} is larger than the measurements by about 120–160 ps.

Discrepancies between simulated and experimental results may result from the not completely accurate CH material parameters, the original CH foam density ρ_0, the Au material parameters, and the radiation source. In this work, the CH foam is treated as a uniform plasma, because our theoretical estimation shows that the pores in the CH foam close within 50 ps after it was heated by the radiation, and this pore closure time is much shorter than the radiation source duration of about 2 ns.

The sensitivity of the flux out of the CH foam to the CH properties is also assessed in this work. On comparing the current CH opacity and EOS with the results from other models at typical CH densities, it is found that the maximum difference between the current material parameters and the results from other models is about 10% when the temperature is below 240 eV. Simulations show that a 10% difference in the CH material parameters can lead to a 1% difference in F_{max} and a 10 ps difference in t_{half}, which are much smaller than the measurement errors. Therefore, the CH material parameters used in our simulations can be considered to be relatively accurate. Furthermore, the Au material parameters have a more significant effect on the propagation of the heat wave within the foam sample. As shown in Fig. 4, the proportion of the radiation fluxes emitted by the Au plasma in the total flux is evidently larger than that of the radiation flux emitted by the CH plasma at 45°, 56°, and 67°, which indicates that the emission behavior of the Au plasma has a strong influence on the measured radiation flux. Thus, the effect of the uncertainty in CH material parameters on the radiation transport process is neglected in the following simulations. Multipliers are introduced to scale ρ_0, the Au material parameters, and the radiation source to better explain the measurements.

B. Obtaining the scaling factors and simulation results using the scaled Au material parameters

The radiation drive temperature is scaled as

$$T_r^{'}(t) = \eta_{\mathrm{src}} T_r(t), \tag{5}$$

where $T_r^{'}(t)$ and $T_r(t)$ are the scaled and original time-dependent radiation drive temperatures, respectively, and η_{src} is the scaling factor of the radiation source, which is independent of time. The density of the CH foam is scaled as

$$\rho_0^{'} = \eta_\rho \rho_0, \tag{6}$$

where $\rho_0^{'}$ and ρ_0 are the scaled and original foam densities, respectively, and η_ρ is the scaling factor of the foam density. In a way similar to that presented in Ref. 17, the Au opacity is scaled by a uniform constant η_{op} as

$$K_{\mathrm{Au}}^{'} = \eta_{\mathrm{op}} K_{\mathrm{Au}}, \tag{7}$$

where $K_{\mathrm{Au}}^{'}$ and K_{Au} are the scaled and original Au opacities, respectively. The Au EOS is adjusted in the same way as adopted in our previous work.[12] Only p_e and ϵ_e are adjusted, while p_i and ϵ_i are kept unchanged. The electron pressure and specific internal energy are given by

TABLE I. Fitting coefficients for the peak radiation flux F_{max} and the breakout time of the heat wave t_{half} of the 1000 and 1500 μm foam cylinders at 45°, 56°, and 67°.

		F_{max}					t_{half}				
Length (μm)	Angle (deg)	α	β	γ	δ	χ^2	α	β	γ	δ	χ^2
1000	45	5.981	−0.130	−0.480	−0.262	4.0×10^{-3}	−1.860	0.053	0.087	0.472	4.1×10^{-5}
	56	6.028	−0.089	−0.508	−0.278	3.9×10^{-3}	−1.804	0.050	0.089	0.464	5.3×10^{-5}
	67	6.038	−0.050	−0.518	−0.306	4.7×10^{-3}	−1.777	0.047	0.091	0.457	5.9×10^{-5}
1500	45	10.908	−0.206	−0.910	−1.624	3.1×10^{-3}	−2.110	0.054	0.113	0.643	1.6×10^{-4}
	56	10.299	−0.113	−0.882	−1.071	8.7×10^{-3}	−2.389	0.071	0.140	0.815	7.2×10^{-4}
	67	9.950	−0.047	−0.866	−0.893	1.3×10^{-2}	−2.553	0.080	0.157	0.880	8.5×10^{-4}

$$p_e = \frac{1}{\lambda}\frac{\partial \ln U_e}{\partial V}, \tag{8}$$

$$\epsilon_e = -\frac{\partial \ln U_e}{\partial \lambda}, \tag{9}$$

where U_e is the electron partition function, $\lambda = (kT_e)^{-1}$, and k is Boltzmann's constant. In our EOS scaling method, U_e is adjusted as

$$U_e^{'} = U_e^{\eta_{\rm eos}}, \tag{10}$$

where $U_e^{'}$ is the adjusted partition function and $\eta_{\rm eos}$ is the EOS scaling factor. In a nearly independent system, this treatment is equivalent to adjusting the particle number of the system. With Eq. (10), p_e and ϵ_e become

$$p_e^{'} = \eta_{\rm eos} p_e, \tag{11}$$

$$\epsilon_e^{'} = \eta_{\rm eos} \epsilon_e, \tag{12}$$

where $p_e^{'}$ and $\epsilon_e^{'}$ are the scaled quantities.

Owing to limited computational resources, a series of simulations are performed corresponding to certain values of $\eta_{\rm src}$, $\eta_{\rm op}$, $\eta_{\rm eos}$, and η_ρ, and then $F_{\rm max}$ and $t_{\rm half}$ are fitted to the following function of these scaling factors:

$$F = F_0 \eta_{\rm src}^{\alpha} \eta_{\rm op}^{\beta} \eta_{\rm eos}^{\gamma} \eta_\rho^{\delta}, \tag{13}$$

where F represents the characteristic quantity $F_{\rm max}$ or $t_{\rm half}$, F_0 represents the value of the corresponding characteristic quantity obtained using LARED-R from the original Au material parameters and radiation source (with all the scaling factors equal to 1), and α, β, γ, and δ are fitting coefficients. Based on Eq. (13), in the ranges $\eta_{\rm src} \in [0.964, 1.036]$, $\eta_{\rm op} \in [0.5, 1.5]$, $\eta_{\rm eos} \in [0.5, 1.5]$, and $\eta_\rho \in [0.969, 1.031]$, we obtain the fitting coefficients for $F_{\rm max}$ and $t_{\rm half}$ of the 1000 and 1500 μm foam cylinders at 45°, 56°, and 67° as listed in Table I. The fitting data include 39 simulated results from different scaling factors. To check our fitting, two testing simulations are performed for the 1000 and 1500 μm foam cylinders, respectively, the results of which are not included in the fitting data. In all the simulations, the scaling factors are randomly selected in the ranges given above. With the superscripts "simu" and "fit" indicating results derived from numerical simulations and from Eq. (13), respectively, Fig. 5 displays (a) $F_{\rm max}^{\rm simu}$ vs $F_{\rm max}^{\rm fit}$ and (b) $t_{\rm half}^{\rm simu}$ vs $t_{\rm half}^{\rm fit}$ at 45°, 56°, and 67° for the 1000 μm (blue solid triangles) and 1500 μm (black solid squares) foam cylinders. The function $y = x$ that represents a perfect fit is shown in red. In Fig. 5, almost all the fitting data points are located on the associated red solid line, suggesting that Eq. (13) describes the dependence of $F_{\rm max}$, and $t_{\rm half}$ on the scaling factors $\eta_{\rm src}$, $\eta_{\rm op}$, $\eta_{\rm eos}$, and η_ρ very well. Data points from the two testing simulations (green and cyan solid circles for the 1000 and 1500 μm foam cylinders, respectively) are also located on the red lines, which means that Eq. (13) can predict the radiation transport processes without simulations.

As shown in Table I, the values of α, β, γ, and δ for the 1500 μm foam are larger than those for the 1000 μm foam, indicating that the radiation fluxes of the 1500 μm foam are more sensitive to the radiation source, material properties, and foam density than those of the 1000 μm foam. Therefore, the fluctuations of experimental data for

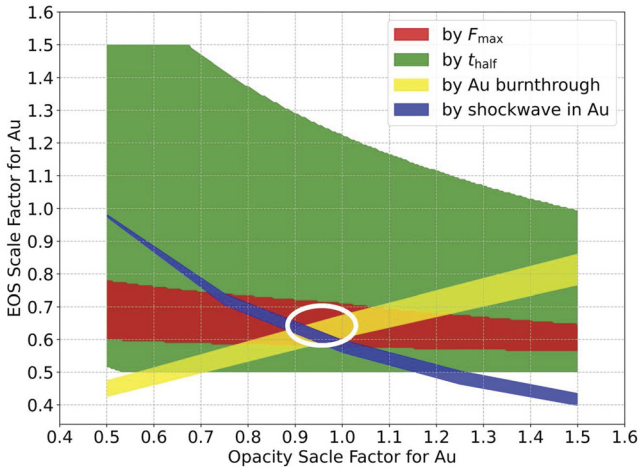

FIG. 6. Ranges of Au opacity and EOS scaling factors $\eta_{\rm op}$ and $\eta_{\rm eos}$ fixed by different experiments. The red band denotes the range of ($\eta_{\rm op}$, $\eta_{\rm eos}$) determined by $F_{\rm max}$, the green band denotes the range of ($\eta_{\rm op}$, $\eta_{\rm eos}$) determined by $t_{\rm half}$, the yellow band shows the range of ($\eta_{\rm op}$, $\eta_{\rm eos}$) fixed by our previous foam-confined plasma expansion experiment,[12] and the blue band shows the range of ($\eta_{\rm op}$, $\eta_{\rm eos}$) fixed by an Au foil burnthrough experiment.[21] The region of overlap of the four bands is marked by the white oval.

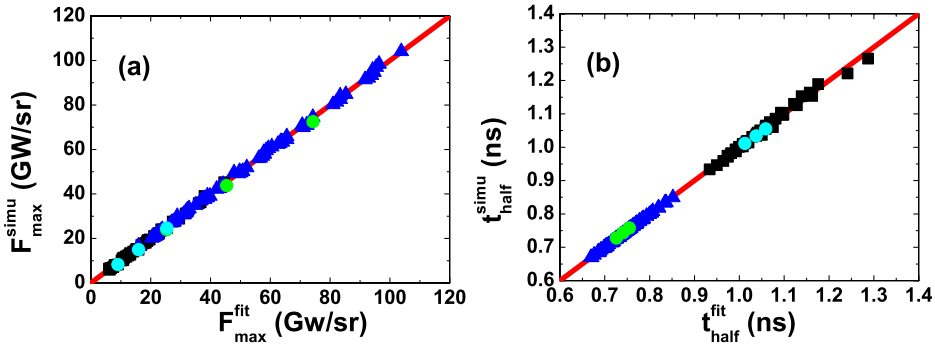

FIG. 5. Plots of (a) $F_{\rm max}^{\rm simu}$ vs $F_{\rm max}^{\rm fit}$ and (b) $t_{\rm half}^{\rm simu}$ vs $t_{\rm half}^{\rm fit}$ at 45°, 56°, and 67° for the 1000 μm (blue solid triangles) and 1500 μm (black solid squares) foam cylinders. The function $y = x$ that represents a perfect fit is shown in red. The green and cyan solid circles correspond to the testing simulations for the 1000 and 1500 μm foam cylinders, respectively.

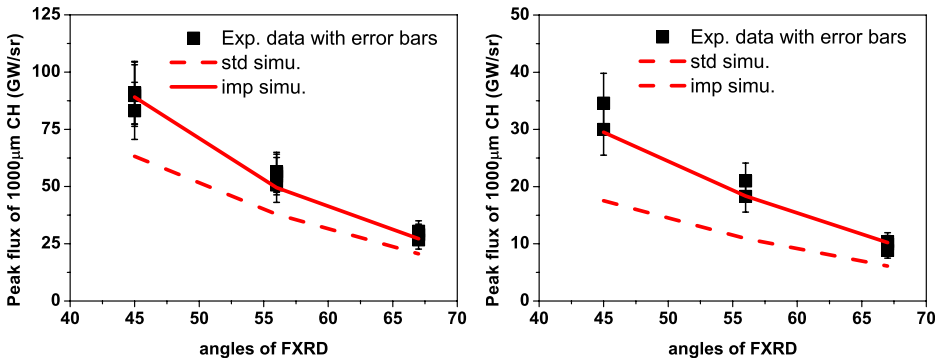

FIG. 7. Comparisons of the angular dependence of the peak fluxes out of the 1000 μm (a) and 1500 μm (b) foams between experiment (black solid squares) and simulations. The red dashed and solid lines show the simulated results calculated using the original and scaled Au material parameters, respectively.

the 1500 μm foam are obviously larger than those for the 1000 μm foam, as shown in Fig. 3.

With the fitting coefficients α, β, γ, and δ in Eq. (13) fixed, an experimental value of $F_{\max}$ or t_{half} can determine a relationship between η_{src}, η_{op}, η_{eos}, and η_{ρ}. For given radiation source, foam density, and experimental values, the relationship between η_{src}, η_{op}, η_{eos}, and η_{ρ} is reduced to a relationship between η_{op} and η_{eos}, which corresponds to a curve in η_{op}–η_{eos} space. Since uncertainties of 3.6%, 3.1%, 100 ps, and 15% exist in the measured T_r, ρ_0, t_{half}, and $F_{\max}$, respectively, the relationship between η_{op} and η_{eos} corresponds to a band in η_{op}–η_{eos} space. Next, we give a detailed description of our method for determining this band. With θ representing one of the angles 45°, 56°, and 67°, and G^{θ} representing the characteristic quantity $F_{\max}$ or t_{half} at θ, we can use available experimental data to define the range of G^{θ} as $[G_2^{\theta}, G_1^{\theta}]$, where

$$G_1^{\theta} = \bar{G}^{\theta} + \Delta G^{\theta}, \tag{14}$$

$$G_2^{\theta} = \bar{G}^{\theta} - \Delta G^{\theta}, \tag{15}$$

with

$$\Delta G^{\theta} = \sqrt{\sigma_{GM}^2 + \sigma_{GF}^2 - \sigma_{GR}^2}, \tag{16}$$

$$\sigma_{GF} = \frac{G_{\max}^{\theta} - G_{\min}^{\theta}}{C}. \tag{17}$$

Here, $\bar{G}^{\theta}$, $G_{\max}^{\theta}$, and $G_{\min}^{\theta}$ are the arithmetic mean, the maximum, and the minimum of G^{θ}, respectively, from available experimental shots. σ_{GM} is the standard deviation of G^{θ} measured in each shot (~15%$F_{\max}$ for $F_{\max}$ and ~100 ps for t_{half}), containing both random and systematic flux measurement errors. σ_{GF} is the standard deviation of G^{θ} measured in different shots, including the random error due to laser and target variations and to random flux measurement error. σ_{GF} is obtained from the range of G^{θ} by the range approach[29] via Eq. (17), where the range coefficient C equals 1.13, 1.64, and 2.06 for the cases with two, three, and four different measured results, respectively. σ_{GR} is the random error of the measured G^{θ}(~2%$F_{\max}$ for $F_{\max}$ and ~10 ps for t_{half}), which is double-counted in σ_{GM} and σ_{GF} and so is subtracted in Eq. (16). ΔG^{θ} describes the total uncertainty of G, including uncertainties in measurements and fluctuations in different shots. Then, with the uncertainties in the measured T_r and ρ_0 fixed at 3.6% and 3.1%, respectively, four curves g_1, g_2, g_3, and g_4 in η_{op}–η_{eos} space are determined by using four groups of (G^{θ}, η_{src}, η_{ρ}): (G_1^{θ}, 0.964, 1.031), (G_1^{θ}, 1.036, 0.969), (G_2^{θ}, 0.964, 1.031), and (G_2^{θ}, 1.036, 0.969). With the regions encompassed by (g_1, g_2) and (g_3, g_4) denoted by the sets A^{θ} and B^{θ}, their union $C^{\theta} = A^{\theta} \cup B^{\theta}$ describes the range of (η_{op}, η_{eos}) determined by G^{θ}. Finally, the intersection $C^{45^{\circ}} \cap C^{56^{\circ}} \cap C^{67^{\circ}}$ describes the range of (η_{op}, η_{eos}) determined by the characteristic quantity G, corresponding to the aforementioned band in η_{op}–η_{eos} space.

The ranges of the Au opacity and EOS scaling factors η_{op} and η_{eos} fixed by this experiment are displayed in Fig. 6. The red band denotes the range of (η_{op}, η_{eos}) determined by $F_{\max}$, and the green band denotes the range of (η_{op}, η_{eos}) determined by t_{half}. We also plot the ranges of η_{op} and η_{eos} fixed in our previous work,[12] where the yellow band shows the range fixed by a foam-confined plasma expansion experiment.[12,19] The blue band shows the range fixed by an Au foil burnthrough experiment.[21] It should be noted that the four bands partially overlap, which suggests that the key physical factors in this experiment have been included, as well as providing a further demonstration of the theoretical approach proposed in our previous work.[12]

The center of the region of overlap is located at approximately (η_{op} = 0.95, η_{eos} = 0.65). Employing the scaled Au opacity and EOS parameters corresponding to (η_{op} = 0.95, η_{eos} = 0.65), we perform numerical simulations again. Figure 7 shows comparisons of the angular dependence of the peak fluxes out of the 1000 and 1500 μm foams between experiment (black solid squares) and simulations. The red dashed and solid lines show the simulated results calculated using the original and scaled Au material parameters, respectively. It can be seen that the results calculated using the scaled Au material parameters agree better with the experimental data. In Fig. 8, we present a comparison of the radiation fluxes out of the 1000 μm [(a)–(c)] and 1500 μm [(d)–(f)] foam cylinders at 45°, 56°, and 67° between the simulated results with scaled (shown in green) and original (shown in red) Au material parameters and the experimental measurements (shown in black). From this figure, we can also see that the simulated fluxes drop faster than the experimental data, which suggests that the simulated cooling process of the foam and Au sleeve

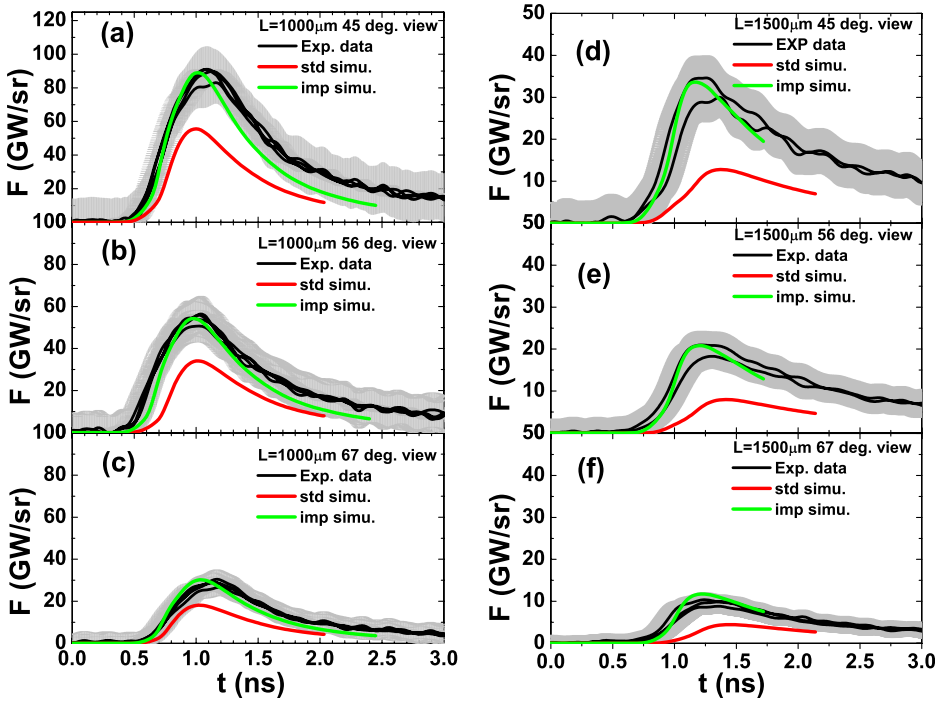

FIG. 8. Comparisons of the radiation fluxes out of the 1000 μm [(a)–(c)] and 1500 μm [(d)–(f)] foam cylinders at (a) and (d) 45°, (b) and (e) 56°, and (c) and (f) 67° between simulations and measurements. The black solid lines show the time profiles of the radiation fluxes measured with FXRDs from different shots. The red and green solid lines show the results calculated using the original and scaled Au material parameters, respectively.

is faster than the experimental process. This phenomenon will be studied in our future work.

IV. CONCLUSIONS

In summary, the radiation fluxes out of CH foam cylinders at different angles have been analyzed theoretically to explain measurements in radiation transport experiments. Owing to the difficulty in validating the Au material parameters and to uncertainties in T_r and ρ_0, multipliers have been introduced to scale the Au material parameters, T_r, and ρ_0 in our simulations. The dependences of $F_{\max}$ and t_{half} on η_{src}, η_{op}, η_{eos}, and η_ρ have been explored via a combination of numerical simulations and fitting. Then, with the uncertainties in the measured T_r and ρ_0 fixed at 3.6% and 3.1%, respectively, the ranges of η_{op} and η_{eos} have been determined by using experimental data as fiducial values. It is found that the ranges of η_{op} and η_{eos} fixed by this experiment overlap partially with those in Ref. 12, which suggests that the key physical factors in this experiment have been included, as well as providing a further demonstration of our theoretical approach proposed previously in Ref. 12. Based on the scaled opacity and EOS parameters, $F_{\max}$ and t_{half} obtained via numerical simulations are in good agreement with the measurements, and their maximum errors are smaller than the measurement uncertainties. These opacity and EOS scaling factors can be used in radiation hydrodynamic simulations within the appropriate drive temperature regions.

ACKNOWLEDGMENTS

This work was supported by the National Key R&D Program of China under Grant No. 2017YFA0403200.

AUTHOR DECLARATIONS

Conflict of Interest

The authors have no conflicts of interest to disclose.

DATA AVAILABILITY

The authors confirm that some data used in Fig. 6 of this study are reproduced from Physics of Plasmas 20, 092704 (2013), with the permission of AIP Publishing.

REFERENCES

[1]N. B. Meezan, M. J. Edwards, O. A. Hurricane, P. K. Patel, D. A. Callahan, W. W. Hsing, R. P. J. Town, F. Albert, P. A. Amendt, L. F. Berzak Hopkins, D. K. Bradley, D. T. Casey, D. S. Clark, E. L. Dewald, T. R. Dittrich, L. Divol, T. Döppner, J. E. Field, S. W. Haan, G. N. Hall, B. A. Hammel, D. E. Hinkel, D. D. Ho, M. Hohenberger, N. Izumi, O. S. Jones, S. F. Khan, J. L. Kline, A. L. Kritcher, O. L. Landen, S. LePape, T. Ma, A. J. MacKinnon, A. G. MacPhee, L. Masse, J. L. Milovich, A. Nikroo, A. Pak, H.-S. Park, J. L. Peterson, H. F. Robey, J. S. Ross, J. D. Salmonson, V. A. Smalyuk, B. K. Spears, M. Stadermann, L. J. Suter, C. A. Thomas, R. Tommasini, D. P. Turnbull, and C. R. Weber, "Indirect drive ignition at the National Ignition Facility," Plasma Phys. Controlled Fusion **59**, 014021 (2017).

[2]R. E. Marshak, "Effect of radiation on shock wave behavior," Phys. Fluids **1**, 24 (1958).

[3]J. D. Lindl, P. Amendt, R. L. Berger, S. G. Glendinning, S. H. Glenzer, S. W. Haan, R. L. Kauffman, O. L. Landen, and L. J. Suter, "The physics basis for ignition using indirect-drive targets on the National Ignition Facility," Phys. Plasmas **11**, 339 (2004).

[4]A. B. R. Cooper, M. B. Schneider, S. A. MacLaren, A. S. Moore, P. E. Young, W. W. Hsing, R. Seugling, M. E. Foord, J. D. Sain, M. J. May, R. E. Marrs, B. R. Maddox, K. Lu, K. Dodson, V. Smalyuk, P. Graham, J. M. Foster, C. A. Back, and J. F. Hund, "Streaked radiography of an irradiated foam sample on the National Ignition Facility," Phys. Plasmas **20**, 033301 (2013).

[5]A. S. Moore, A. B. R. Cooper, M. B. Schneider, S. MacLaren, P. Graham, K. Lu, R. Seugling, J. Satcher, J. Klingmann, A. J. Comley, R. Marrs, M. May, K. Widmann, G. Glendinning, J. Castor, J. Sain, C. A. Back, J. Hund, K. Baker, W. W. Hsing, J. Foster, B. Young, and P. Young, "Radiation transport and energetics of laser-driven half-hohlraums at the National Ignition Facility," Phys. Plasmas **21**, 063303 (2014).

[6]D. Mihalas and B. W. Mihalas, *Foundations of Radiation Hydrodynamics* (Academic, New York, 1966).

[7]G. C. Pomraning, *The Equations of Radiation Hydrodynamics* (Pergamon Press, London, 1973).

[8]Y. B. Zeldovich and Y. P. Raizer, *Physics of Shock Waves and High Temperature Hydrodynamics Phenomena* (Academic, New York, 1984).

[9]J. Li, J. Li, and G. Meng, "Reversal of Hugoniot Iocus for strong shocks due to radiation," Phys. Plasmas **18**, 042301 (2011).

[10]A. Mizuta, J. O. Kane, M. W. Pound, B. A. Remington, D. D. Ryutov, and H. Takabe, "Formation of pillars at the boundaries between H II regions and molecular clouds," Astrophys. J. **647**, 1151 (2006).

[11]J. H. Hammer and M. D. Rosen, "A consistent approach to solving the radiation diffusion equation," Phys. Plasmas **10**, 1829 (2003).

[12]G. Meng, J. Li, J. Yang, T. Zhu, S. Zou, M. Wang, and W. Zhang, "A simple method to verify the opacity and equation of state of high-Z plasmas," Phys. Plasmas **20**, 092704 (2013).

[13]O. A. Hurricane and J. H. Hammer, "Bent Marshak waves," Phys. Plasmas **13**, 113303 (2006).

[14]G. Meng, J. Wang, X. Wang, J. Li, and W. Zhang, "Generation of a sharp density increase in radiation transport between high-Z and low-Z plasmas," Matter Radiat. Extremes **1**, 249 (2016).

[15]T. Shussman and S. I. Heizler, "Full self-similar solutions of the subsonic radiative heat equations," Phys. Plasmas **22**, 082109 (2015).

[16]C. A. Back, J. D. Bauer, J. H. Hammer, B. F. Lasinski, R. E. Turner, P. W. Rambo, O. L. Landen, L. J. Suter, M. D. Rosen, and W. W. Hsing, "Diffusive, supersonic x-ray transport in radiatively heated foam cylinders," Phys. Plasmas **7**, 2126 (2000).

[17]T. M. Guymer, A. S. Moore, J. Morton, J. L. Kline, S. Allan, N. Bazin, J. Benstead, C. Bentley, A. J. Comley, J. Cowan, K. Flippo, W. Garbett, C. Hamilton, N. E. Lanier, K. Mussack, K. Obrey, L. Reed, D. W. Schmidt, R. M. Stevenson, J. M. Taccetti, and J. Workman, "Quantifying equation-of-state and opacity errors using integrated supersonic diffusive radiation flow experiments on the National Ignition Facility," Phys. Plasmas **22**, 043303 (2015).

[18]W. Shang, T. Zhu, T. Song, W. Zhang, Y. Zhao, G. Xiong, J. Zhang, and J. Yang, "Study of x-ray radiant characteristics and thermal radiation redistribution in CH foam filling cylindrical cavities," Phys. Plasmas **18**, 042705 (2011).

[19]J. Yang, G. Meng, T. Zhu, J. Zhang, J. Li, X. He, R. Yi, Y. Xu, Z. Hu, Y. Ding, S. Liu, and Y. Ding, "Experimental study of the hydrodynamic trajectory of an x-ray-heated gold plasmas," Phys. Plasmas **17**, 062702 (2010).

[20]O. Willi, L. Barringer, C. Vickers, and D. Hoarty, "Study of super- and subsonic ionization fronts in low-density, soft X-ray-irradiated foam targets," Astrophys. J., Suppl. Ser. **127**, 527 (2000).

[21]C. Wu, The simulation of gold ablation experiment on Shenguang III prototype in 2007, GFA011864G, 2008.

[22]C. Huang and X. Luo, The fabrication standard of low-density PMP foams, Internal Report of Laser Fusion Research Center, 2015gh-1221-02, 2015.

[23]Z. Li, X. Jiang, S. Liu, T. Huang, J. Zheng, J. Yang, S. Li, L. Guo, X. Zhao, H. Du, T. Song, R. Yi, Y. Liu, S. Jiang, and Y. Ding, "A novel flat-response x-ray detector in the photon energy range of 0.1–4 keV," Rev. Sci. Instrum. **81**, 073504 (2010).

[24]D. Yang, Z. Li, L. Guo, S. Li, R. Yi, T. Song, H. Zhang, Z. Wang, X. Jiang, S. Jiang, and Y. Ding, "The influence of laser clipped by the laser entrance hole on hohlraum radiation measurement on Shenguang-III prototype," Rev. Sci. Instrum. **85**, 033504 (2014).

[25]T. Feng, "A numerical method for solving radiation transport equation on Lagrangian mesh," Chin. J. Comput. Phys. **21**, 427 (2004).

[26]Y. Rong, H. Xudeng, and L. Jinghong, "A two-dimensional cylindric symmetric radiative transfer benchmark model and code tests," Chin. J. Comput. Phys. **27**, 533 (2010).

[27]F. J. D. Serduke, E. Minguez, S. J. Davidson, and C. A. Iglesias, "WorkOp-IV summary: Lessons from iron opacities," J. Quant. Spectrosc. Radiat. Transfer **65**, 527 (2000).

[28]R. M. More, K. H. Warren, D. A. Young, and G. B. Zimmerman, "A new quotidian equation of state (QEOS) for hot dens matter," Phys. Fluids **31**, 3059 (1988).

[29]The Compilation Group of Handbook of Mathematics, *Handbook of Mathematics* (Higher Education Press, Beijing, 1979), pp. 865–866.